

A Gradient Boosted Mixed-Model Machine Learning Framework for Vessel Speed in the U.S. Arctic

Mauli Pant^{a,*}, Linda Fernandez^b, Indranil Sahoo^c

^a*Integrative Life Sciences Doctoral Program, Center for Integrative Life Sciences Education, Virginia Commonwealth University, Richmond, Virginia, USA*

^b*School of Life Sciences and Sustainability, Department of Economics, Virginia Commonwealth University, Richmond, Virginia, USA*

^c*Department of Statistical Sciences and Operations Research, Virginia Commonwealth University, Richmond, Virginia, USA*

Abstract

Understanding how environmental and operational conditions influence vessel speed is crucial for characterizing navigational conditions in the Arctic. We analyzed AIS data from 2010–2019 of vessel speed over ground (SOG). Over half the AIS records showed zero SOG, so treating zero and positive SOG as a continuous process can obscure important patterns. We therefore applied a two-stage machine learning framework, first modeling the probability of $\text{SOG} > 0$, and then modeling SOG conditional on being positive. We integrated AIS observations with sea ice concentration, course over ground, wind, bathymetric depth, distance to coast, vessel group, and navigational status. Gradient boosted decision trees with random effects captured nonlinear environmental responses and repeated observations. The positive SOG classifier achieved strong discrimination ($\text{AUC} \approx 0.85$), while the conditional speed model explained $\approx 77\%$ of out-of-fold variance. SHAP values quanti-

*Corresponding author.

Email address: pantm2@vcu.edu (Mauli Pant)

fied covariate effects by decomposing model predictions into additive contributions from individual variables. Distance to coast and bathymetric depth were dominant determinants of the likelihood and magnitude of vessel speed, while effect of changes in course, vessel group, and navigational status was secondary. Wind and sea ice effects were modest. These results empirically characterize Arctic vessel operating regimes for speed management and corridor level assessment.

Keywords: Arctic shipping; Automatic Identification System (AIS); Environmental drivers; Gaussian Process; GPBoost; Spatial effects; Speed Over Ground (SOG).

1. Introduction

The Arctic presents one of the most challenging maritime environments in the world. Shifting sea ice, high winds, and complex bathymetric depth create conditions where safe and efficient navigation requires constant attention. These challenges are intensifying as climate change reduces sea ice extent, increasing seasonal vessel traffic while raising concerns about navigational safety. According to the ten-year forecast report (U.S. Committee on the Marine Transportation System, 2019), Arctic vessel traffic could be three times higher in 2030 than in 2008. Because vessel speed influences navigation risk, exposure time in sensitive habitats, and the severity of environmental effects, understanding the drivers of observed speed over ground (SOG) is central to Arctic navigation management.

Much of the existing literature emphasizes analytical modeling approaches, with comparatively few studies leveraging empirical or statistical analyses of

observed vessel navigation (Aksenov et al., 2017; Chang et al., 2015; Goerlandt et al., 2017; Kuuliala et al., 2017; Löptien and Axell, 2014; Montewka et al., 2015; Pruyn, 2016). In addition, environmental drivers are typically treated in isolation rather than jointly. This limits the understanding of combined effects of sea ice, wind, and bathymetric depth on vessel speed over ground (SOG), an operational variable central to fuel efficiency, navigational safety, and environmental impact.

Our contribution to the literature involved analyzing Automatic Identification System (AIS) vessel observations from 2010–2019 during the open-water season (July–October), integrated with satellite derived environmental data. By explicitly separating zero and positive speed regimes and modeling their environmental and operational drivers, this study provided an interpretable characterization of Arctic vessel operations and identified where speed related navigational and environmental risks were most likely to arise. The results offer a data driven basis for understanding how spatial context and steering shape vessel speed under increasing Arctic vessel traffic.

While ice-related speed thresholds provide a useful baseline for identifying potentially hazardous operating conditions (Figure A1), observed vessel speeds in the U.S. Arctic exhibited substantial variability even under similar ice conditions (Figure 2). This variability indicates that vessel speed decisions during the open water navigation season were shaped by a broader set of environmental and operational constraints beyond ice alone. In particular, bathymetric depth, proximity to shore, wind conditions, and vessel specific navigational status interacted to influence SOG across space and time. As a result, threshold based ice risk metrics, while operationally informative, can-

not capture the nonlinear and multivariate drivers of Arctic vessel navigation observed in practice.

This study addressed these limitations by embedding ice related navigation risk within a data driven modeling framework that explicitly accounted for environmental, spatial, and operational drivers of vessel speed. To this end, we employed a tree based gradient boosting framework with structured random effects. This modeling approach is well suited for capturing nonlinear relationships, threshold effects, and heterogeneous vessel operations in large scale AIS data (Chen and Guestrin, 2016; Ke et al., 2017; Sigrist, 2021). By integrating more than a decade of AIS observations with environmental covariates, our approach extended existing ice risk frameworks from static metrics toward a statistical characterization of vessel navigation under varying environmental conditions.

Tree-based machine learning models have been widely applied to AIS data for vessel navigation analysis, including vessel speed prediction, characterization of speed distributions, and identification of low speed or zero speed operating contexts in coastal waters (Ma et al., 2024; Wang et al., 2022; Yang et al., 2024). These studies demonstrate the predictive flexibility of ensemble tree methods but typically treat vessel speed as a single continuous process and do not explicitly address the strong zero inflation in SOG. Such approaches also rarely account for repeated observations within vessels, locations, or time periods, limiting their utility for policy relevant interpretation of vessel operating regimes. Furthermore, environmental drivers such as sea ice, bathymetric depth, and wind are often incorporated only in limited form or excluded entirely, constraining physical interpretation of model outputs.

This study advances the existing literature by introducing a unified framework that treats zero and positive vessel speeds as distinct operating regimes rather than a single continuous process. By separating stationary behavior ($SOG = 0$) from active navigation ($SOG > 0$), the analysis distinguishes stopping, maneuvering, and sustained transit patterns that are otherwise conflated in AIS-based speed models. Environmental and spatial drivers, including sea ice concentration, bathymetric depth, distance to coast, and wind forcing, are incorporated jointly, allowing nonlinear responses and interactions to be resolved across operating regimes. The framework further accounts for repeated observations within vessels, spatial grid cells, and daily time periods through structured random effects, capturing persistent operational and geospatial constraints on vessel speed.

To interpret the fitted machine learning models, we employ SHapley Additive exPlanations (SHAP; Lundberg and Lee, 2017) framework, which takes a game theoretic approach to explaining the output of a machine learning model. Shapley values provide a principled framework for fairly attributing a model’s prediction to individual features by averaging their marginal contributions across all possible feature coalitions. When applied to machine learning models, this yields additive, locally consistent explanations that decompose each prediction relative to a baseline, enabling interpretable assessment of nonlinear effects and feature interactions in complex black-box models (Wikle et al., 2023). This approach facilitates examination of environmental and operational drivers of vessel speed across heterogeneous Arctic navigation contexts using large-scale AIS data, characterizing observed vessel speeds as the outcome of interacting environmental, spatial, and operational

processes.

2. AIS Vessel Traffic Data and Environmental Covariates

Vessel traffic data are transmitted via an onboard Automatic Identification System (AIS) transponder, which communicates vessel location and identity to other vessels and coastal authorities. These data are recorded for vessels navigating U.S. coastal waters and are distributed by the U.S. Coast Guard through the AIS platform (<https://marinecadastre.gov/AIS/>), which is jointly managed by the Bureau of Ocean Energy Management (BOEM), the National Oceanic and Atmospheric Administration (NOAA), and the U.S. Coast Guard Navigation Center. AIS records are available from 2009 onward; in this study, we focused on the period 2010–2019.

Analysis was restricted to July–October, coinciding with the Arctic shipping season, and to a spatial extent defined by longitude ($-138^{\circ}, -172^{\circ}$) and latitude ($66.6^{\circ}, 72.5^{\circ}$) within the U.S. Arctic. Missing values in vessel attributes were supplemented where possible; residual gaps were imputed using vessel type means. Across 2010–2019, a total of 14,789,591 AIS observations were retained for July–October within the defined spatial extent. Tug/tow vessels accounted for the highest volume of observations, followed by cargo and other categories. Cruise ships exhibited the highest average SOG, whereas cargo, tanker, and search and rescue (SAR) vessels represented the largest and heaviest groups.

The empirical distribution of SOG was highly left skewed, with the majority of observations concentrated near zero. More than half (53%) of all AIS records reported a speed of exactly 0 knots, indicating strong zero inflation

in vessel SOG. This characteristic has direct implications for model specification, as the data combine frequent zero SOG observations with a continuous distribution of positive SOG values. Table 1 summarizes the composition of AIS observations by vessel group conditional on zero or positive SOG. Tug and tow vessels dominated both categories, reflecting their extensive presence in the study region, but accounted for a substantially larger share of zero SOG observations. In contrast, cargo vessels represented a higher proportion of positive SOG observations. High speed craft were disproportionately represented among zero SOG observations.

Additional patterns emerged when AIS records were stratified by navigation status (Table 2). Most positive SOG observations corresponded to vessels under way using engine, while zero SOG observations were more frequently associated with anchoring, mooring, and undefined operational statuses. Together, Tables 1 and 2 show that zero SOG AIS observations spanned many vessel groups and navigation statuses. This heterogeneity has important implications for modeling vessel speed and motivated the use of a two-stage framework that distinguishes zero SOG observations from positive SOG values.

Figure 1 shows that sea ice concentration was high for both zero SOG and positive SOG observations. In contrast, distance to coast clearly differentiated the two, with zero SOG observations concentrated much closer to shore. Wind conditions were similar for zero SOG and positive SOG observations, although their distributions differed modestly. Vessels with both zero and positive SOG were observed across shallow and deep waters.

Table 1: Distribution of AIS observations by vessel group and Zero Inflation (July-October, 2010-2019). Percentages are calculated within each category ($SOG = 0$ or $SOG > 0$).

Vessel Group	Positive ($SOG > 0$)		Zero ($SOG = 0$)	
	Count	%	Count	%
Tug / Tow	4,401,128	63.23	5,791,372	73.97
Cargo	1,051,955	15.11	921,494	11.77
Other	971,605	13.96	404,417	5.17
Fishing	209,847	3.02	132,906	1.70
High-Speed Craft	38,486	0.55	346,506	4.43
Tanker	78,541	1.13	108,931	1.39
Pleasure Craft	68,084	0.98	12,603	0.16
Passenger	19,872	0.29	9,424	0.12
Cruise Ship	5,253	0.08	13,636	0.17
SAR	12,712	0.18	328	0.00
Unspecified	88,392	1.27	65,646	0.84
Other Specialized [†]	15,526	0.22	22,280	0.29

[†]Includes anti pollution vessels, dredgers, pilot vessels, service ships, reserved categories, and other low frequency vessel types.

Table 2: Distribution of AIS observations by navigation status and Zero Inflation (July-October, 2010-2019). Percentages are calculated within each category ($SOG = 0$ or $SOG > 0$).

Navigation Status	Positive ($SOG > 0$)		Zero ($SOG = 0$)	
	Count	%	Count	%
Status 0	5,520,374	79.32	5,949,981	75.99
Status 1	488,561	7.02	482,709	6.17
Status 3	374,897	5.39	198,430	2.53
Status 15	191,891	2.76	552,046	7.05
Status 5	146,743	2.11	315,647	4.03
Status 11	124,458	1.79	228,830	2.92
Status 12	56,595	0.81	49,357	0.63
Status 8	49,176	0.71	27,012	0.35
Status 2	3,310	0.05	21,058	0.27
Status 6	2,272	0.03	4,459	0.06
Status 7	1,239	0.02	—	—

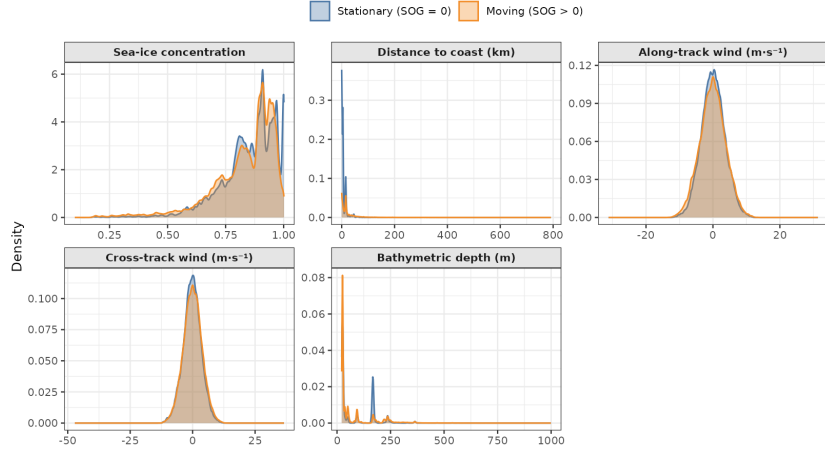


Figure 1: Distribution of environmental and spatial covariates by Zero or positive SOG (July-October, 2010-2019). Density curves compare SOG = 0 and SOG > 0 AIS observations. Wind effect is represented using along-track and cross-track components ($\text{m}\cdot\text{s}^{-1}$), consistent with the regression specification. Axes are shown on variable specific scales to emphasize within variable distributional differences.

The following environmental variables were extracted and collocated with AIS positions on a $0.5^\circ \times 0.5^\circ$ grid at daily resolution:

- **Sea ice concentration.** Daily sea ice concentration fields were obtained from the NOAA OISST/DOISST high-resolution blended analysis NetCDF products (icec.day.mean.YYYY.nc; variable icec) for 2010–2019. These fields are distributed with the OISST/DOISST product and use external sea-ice analyses (NCEP and NASA GSFC), as documented in the dataset metadata and described by (Huang et al., 2021). Ice concentration was reported on a latitude–longitude grid at a spatial resolution of 0.25° and expressed as a unitless fractional ice cover (0–1). NetCDF time stamps were converted to calendar dates using the native time encoding (days since 1800-01-01, UTC), and longitudes were wrapped to $[-180^\circ, 180^\circ]$ for consistency with AIS coordinates. Ice fields were

subset to the U.S. Arctic study domain ($66.6\text{--}72.5^\circ\text{N}$; $172\text{--}138^\circ\text{W}$) and subsequently aggregated to a 0.5° grid using spatial averaging to align with the resolution of environmental covariates mapped to vessel observations.

Sea ice concentration was collocated with AIS positions by assigning each AIS record to the nearest daily ice date and extracting ice values at vessel locations. For each day, the ice field was rasterized to a $0.5^\circ \times 0.5^\circ$ grid (EPSG:4326) using the mean ice concentration within each grid cell, and vessel level ice values were obtained by spatial extraction from this raster. When extraction returned missing values (e.g., due to gaps in the gridded ice field), missing ice values were imputed using a two step geostatistical procedure. First, missing values in the daily ice field were filled using inverse distance weighting (IDW; $n_{\max} = 10$, power parameter $p = 2$). Second, an empirical variogram was estimated from the filled daily ice field and a spherical variogram model was fitted; ordinary kriging with $n_{\max} = 10$ neighbors was then used to predict ice concentration at AIS locations for that day. This procedure ensured complete ice covariate coverage for all AIS observations used in the modeling.

- **Wind and bathymetry.** Daily gridded fields of 10-m wind components and bathymetric depth (Copernicus Climate Change Service (C3S), 2024) were collocated with AIS positions using the same day matching procedure applied to sea ice concentration. Environmental fields were provided at daily temporal resolution and mapped to a common $0.5^\circ \times 0.5^\circ$ latitude-longitude grid (EPSG:4326), matching

the spatial resolution used for AIS covariates. For each day, AIS time stamps were assigned to the nearest available daily environmental field.

Wind direction was represented by the eastward and northward 10-m wind components, denoted u_{10} and v_{10} (m s^{-1}), and bathymetric depth was denoted wmb (m). For each day, environmental fields were rasterized to the $0.5^\circ \times 0.5^\circ$ grid using mean aggregation within grid cells, and initial vessel level covariate values were obtained by bilinear extraction from the daily rasters.

To ensure complete covariate coverage at vessel locations and to reduce the effects of assigning identical grid-cell values in the daily environmental fields, wind and bathymetry were interpolated to vessel positions using ordinary kriging, applied separately for u_{10} , v_{10} , and wmb on each day. For each variable, duplicated spatial points were removed, an empirical variogram was computed, and a parametric variogram model was fitted prior to kriging to AIS locations using up to $n_{\max} = 10$ neighboring points. An exponential variogram model was used for u_{10} , while Gaussian variogram models were used for v_{10} and wmb. The resulting kriged predictions were assigned as the final vessel level covariate values for that day.

Interpolation was used solely to ensure complete covariate coverage and did not introduce new vessel observations.

Figure 2 presents a synthesized snapshot of the integrated datasets, illustrating areas of heightened navigational concern where all three datasets overlap within the US Arctic. This visualization highlights the integrative spatial framework developed for this study, which combines vessel volume,

environmental conditions, and ecological factors in a unified analysis.

Spatial overlays of vessel observations, sea ice concentration, and wind conditions show substantial co-occurrence in coastal corridors where persistent ice intersects with shallow shelves and steep depth gradients (Figure 2). We further calculated a binary ice risk indicator by comparing each vessel's observed SOG with a reference safe speed curve derived from the ACCESS (Arctic Climate Change Economy and Society) report (HSVA Arctic Technology, 2014) (see Figure A1), which relates recommended operating speed to sea ice concentration. Risk was assigned a value of 1 when a vessel's SOG exceeded the ACCESS derived safe speed for the corresponding ice concentration, and 0 otherwise. This binary indicator was then aggregated within $0.5^\circ \times 0.5^\circ$ grid cells to estimate the proportion of potentially risky vessel transits at each location. Spatial overlap between elevated ice risk, high vessel density, and shallow bathymetric depth highlights areas where navigational and ecological risks may co-occur, particularly in regions that overlap with sensitive marine mammal habitats (Reeves et al., 2014; Hauser et al., 2018; Halliday et al., 2017).

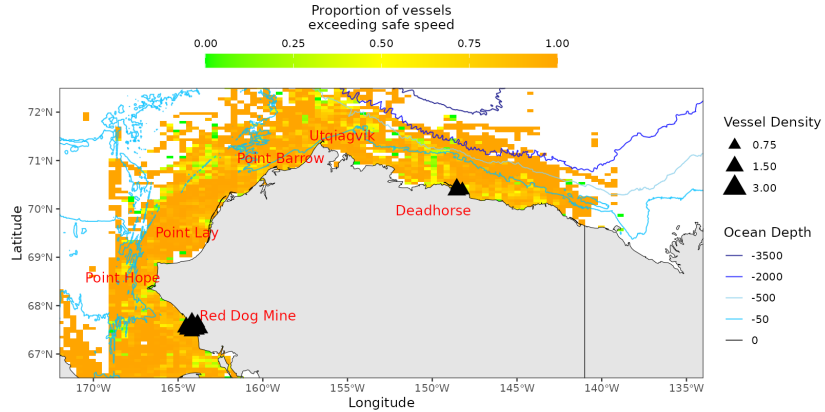


Figure 2: Spatial distribution of binary ice-related speed risk across the U.S. Arctic (July–October, 2010–2019). Grid cell shading indicates the proportion of AIS observations exceeding an ice-dependent safe speed threshold (Figure A1). Black triangles mark the ten highest vessel density locations, scaled by a relative density index. Bathymetric depth contours provide spatial context.

3. Statistical Methodology: A Two-Stage Machine Learning Framework

Vessel SOG was modeled using a two-stage framework consisting of (i) classification of whether a vessel’s SOG was zero or positive and (ii) conditional regression of vessel speed given positive SOG. The two stages were estimated sequentially rather than under a single joint likelihood, separating the stochastic process governing the presence or absence of speed from the process governing speed variability during active navigation.

3.1. GPBoost Modeling Framework

Both stages of the analysis were implemented using the GPBoost framework (Sigrist, 2021), which combines gradient boosted decision trees (GB-

DTs) with grouped Gaussian random effects. Random effects captured correlation from repeated observations within the same vessel (MMSI), grid cell, and day (TimeID), rather than assuming independence. Spatial grouping used a regular $0.5^\circ \times 0.5^\circ$ latitude–longitude grid to align with the resolution of environmental covariates and ensure consistent spatial coverage where data were missing. Temporal grouping was defined at the daily level (TimeID) to account for day-to-day correlation in vessel navigation. This structure allowed separation of systematic covariate effects from vessel specific, spatial, and day to day variability, reducing bias that would arise from treating repeated observations as independent. Further, GPBoost provided a unified modeling architecture for flexible nonlinear covariate effects while explicitly accounting for correlated structure arising from repeated vessel observations across space and time.

For observation i , the latent linear predictor is written as

$$\eta_i = f(\mathbf{x}_i) + u_{g_{\text{mmsi}}(i)} + s_{g_{\text{cell}}(i)} + t_{g_{\text{time}}(i)},$$

where $f(\mathbf{x}_i)$ is an additive ensemble of regression trees, and $u_{g_{\text{mmsi}}(i)}$, $s_{g_{\text{cell}}(i)}$, and $t_{g_{\text{time}}(i)}$ are grouped Gaussian random effects for vessel, spatial grid cell, and time index, respectively. The grouped random effects are modeled as

$$u_v \sim \mathcal{N}(0, \sigma_{\text{MMSI}}^2), \quad s_c \sim \mathcal{N}(0, \sigma_{\text{cell}}^2), \quad t_\tau \sim \mathcal{N}(0, \sigma_{\text{time}}^2),$$

and the boosted tree and random effects components were estimated jointly using the integrated likelihood approach implemented in GPBoost. The non-

linear predictor is constructed as

$$f(\mathbf{x}_i) = \sum_{m=1}^M \alpha T_m(\mathbf{x}_i),$$

where α is the learning rate and each tree T_m is fitted sequentially to residual structure left by the previous ensemble.

The covariate vector is defined as

$$\mathbf{x}_i = \begin{pmatrix} \text{scaled_icec}_i, \text{ scaled_wind_along}_i, \text{ scaled_wind_cross}_i, \\ \text{ scaled_dist_to_coast}_i, \text{ scaled_bathy}_i, \text{ scaled_cog_sin}_i, \\ \text{ scaled_cog_cos}_i, \text{ scaled_}\Delta\text{COG}_i, \text{ VesselGroup}_i, \text{ Status}_i \end{pmatrix}^\top.$$

Sea ice concentration, icec_i , denotes fractional ice cover at observation i (unitless; 0–1), with scaled_icec_i its standardized form. Wind direction is represented by the eastward and northward 10-m wind components (u_{10} , v_{10}), which are rotated relative to each vessel’s course over ground (COG) to obtain along-track and cross-track wind components (m s^{-1}). Distance to coast is measured in kilometers (km), and bathymetric depth represents seafloor depth in meters (m).

Directional effects are represented using a circular encoding of course over ground via its sine and cosine components, scaled_cog_sin_i and scaled_cog_cos_i , which preserve directional continuity at $0/360^\circ$. Short-term steering intensity was captured by the absolute circular change in course, $\text{scaled_}\Delta\text{COG}_i$, measured in degrees between successive AIS observations. Categorical variables VesselGroup_i and Status_i encoded vessel type and navigational status, respectively.

All continuous variables were standardized to zero mean and unit variance, so covariates are unitless and represent relative effects. Categorical variables were encoded as integer indices, and boosted tree effect magnitudes therefore reflect relative importance rather than original units.

3.1.1. Step 1: Binary Classification of Zero and Positive SOG

To account for structured dependence in AIS observations, random intercepts were specified for 530 unique MMSI identifiers, 327 spatial grid cells, and 1,194 daily time indices. For each AIS observation, SOG was used to define a binary indicator

$$Y_i = \begin{cases} 1, & \text{if } \text{SOG}_i > 0, \\ 0, & \text{if } \text{SOG}_i = 0, \end{cases}$$

where $Y_i = 1$ denotes positive SOG and $Y_i = 0$ denotes zero SOG.

In this stage, GPBoost was fitted with a Bernoulli likelihood and a probit link,

$$p_i = \Phi(\eta_i),$$

where $\Phi(\cdot)$ denotes the standard normal cumulative distribution function and η_i is the latent linear predictor combining nonlinear covariate effects and grouped random effects as defined in Section 3.1. The probit link was used because it is compatible with the latent Gaussian mixed-effects formulation underlying GPBoost (Sigrist, 2021).

Across the full dataset, 7,829,481 AIS observations (52.9%) corresponded to zero SOG ($\text{SOG} = 0$), while 6,959,580 observations (47.1%) indicated positive speeds ($\text{SOG} > 0$), resulting in moderate class imbalance. Model

performance was evaluated using stratified K -fold cross-validation with random subsampling of the majority class to address class imbalance. Let $\mathcal{D} = \{(x_i, y_i)\}_{i=1}^N$, with $y_i \in \{0, 1\}$ indicating zero SOG and positive SOG. Within each training fold k , a balanced training set was constructed as

$$\tilde{\mathcal{D}}_{\text{train}}^{(k)} = \mathcal{D}_{\text{train},1}^{(k)} \cup \mathcal{S}\left(\mathcal{D}_{\text{train},0}^{(k)}, |\mathcal{D}_{\text{train},1}^{(k)}|\right),$$

where $\mathcal{S}(\cdot)$ denotes random sampling without replacement. Validation folds retained the original class proportions. This procedure follows standard practice in imbalanced classification (Japkowicz and Stephen, 2002). Majority class subsampling was applied within training folds to stabilize fitting given strong spatial clustering of zero SOG observations nearshore.

3.1.2. Step 2: Conditional Regression of Vessel Speed

The conditional SOG regression was fitted to the moving subset (SOG > 0), comprising 6,959,580 observations from 527 unique vessels (MMSI), 325 spatial grid cells, and 1,191 daily time indices (TimeID). These reduced counts reflect the exclusion of zero-speed records, which removed vessels, grid cells, and days associated solely with zero SOG observations.

Let SOG_i denote the observed SOG for AIS observation i . The continuous response variable for the regression stage is defined as

$$y_i = \sqrt{\text{SOG}_i}, \quad \text{for } Y_i = 1,$$

where the square root transformation was applied to positive SOG values to mitigate right skewness and heteroskedasticity while maintaining a mono-

tonic and physically interpretable relationship with vessel speed. This choice preserves relative differences among moderate and high speeds and avoids excessive compression associated with logarithmic transformations. The transformed speed was modeled as

$$y_i = f(\mathbf{x}_i) + u_{g_{\text{mmsi}}(i)} + s_{g_{\text{cell}}(i)} + t_{g_{\text{time}}(i)} + \varepsilon_i,$$

where ε_i is an observation level error term with mean zero. After accounting for covariate effects and vessel, space, and time specific random effects, the remaining observation level variation was assumed independent and reflected measurement noise and other small scale, unmodeled influences. Tree depth, learning rate, and minimum leaf size were selected using cross-validated performance on the training data, with conservative regularization to prioritize generalization.

4. Model Evaluation

4.1. Evaluation of Binary SOG Classification

Model discrimination was assessed using the area under the receiver operating characteristic curve (AUC) computed from out-of-fold predictions (Figure 3). The overall out-of-fold AUC was 0.845, with fold level values ranging from 0.844 to 0.846 (standard deviation 9.2×10^{-4}), indicating strong and highly stable discrimination between zero SOG and positive SOG observations.

Classification performance at a probability threshold of $\hat{p}_{\text{pos_SOG}} \geq 0.5$ was summarized using a confusion matrix, treating positive SOG observations ($Y_i = 1$) as the positive class. Overall accuracy (0.760), substantially

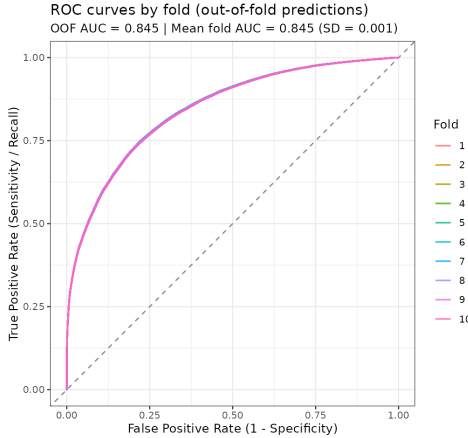


Figure 3: ROC curve with AUC (out-of-fold predictions). The close overlap of curves across folds indicates that classifier performance is robust to spatial, temporal, and vessel level heterogeneity and generalizes well beyond individual training sets.

exceeded the no information rate (0.531). Sensitivity for detecting $SOG > 0$ was 0.703, while specificity for identifying $SOG = 0$ was 0.810, yielding a balanced accuracy of 0.757. Cohen's kappa of 0.516 indicates moderate agreement beyond chance, which is expected in the presence of class imbalance, even when overall discrimination is strong (Feinstein and Cicchetti, 1990). Consistent with this, the high AUC indicates effective separation between zero and positive speed observations. Precision–recall analysis yielded a PR–AUC of 0.845, indicating strong performance in identifying positive SOG vessels while maintaining a low false positive rate (Figure 4). This substantially exceeded the baseline PR–AUC expected from the prevalence of positive SOG observations alone.

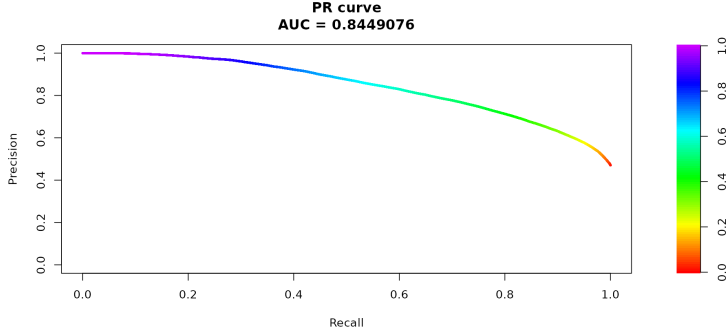


Figure 4: Evaluation of the SOG zero or positive SOG classification model using out-of-fold predictions shows the precision recall curve, with color indicating the decision threshold and illustrating the trade off between precision and recall across operating points.

4.2. Evaluation of Regression

Cross-validation was performed at the level of individual AIS records. Random effects for MMSI, cell, and TimeID were estimated using training data only and were not shared across folds, ensuring that validation predictions were generated without access to validation outcomes. Predictive performance was evaluated using five fold cross-validation, with the GPBoost model trained on a square root transformation of vessel speed ($\sqrt{\text{SOG}}$) and out-of-fold predictions generated for each fold. Performance was stable across folds, with $R^2_{\text{SOG}} \approx 0.77$ and absolute errors near 1 knot (MAE ≈ 1.04 kn; RMSE ≈ 1.77 kn).

Calibration was assessed using out-of-fold predictions by comparing mean observed and predicted speeds within equal frequency bins (Figure 5). The calibration curve closely follows the 1:1 line, indicating minimal bias.

Based on out-of-fold diagnostic summaries, absolute prediction error increased gradually with vessel speed, with mean absolute error remaining below approximately 1.5 knots for the majority of observations ($\text{SOG} \leq 6$

Table 3: Performance metrics for zero or positive SOG classification (positive class = Positive SOG).

Metric	Value
Accuracy	0.760
Balanced Accuracy	0.757
Sensitivity (Recall)	0.703
Specificity	0.810
Precision (PPV)	0.767
Negative Predictive Value	0.754
Cohen's Kappa	0.516
Prevalence (Positive SOG)	0.471
Detection Rate	0.331
Detection Prevalence	0.431

knots) and increasing at higher speeds where data were comparatively sparse. The close agreement between mean and median errors indicates robustness to outliers, while the gradual increase in upper tail error suggests that uncertainty at higher speeds reflects limited data availability rather than systematic model bias.

Table 4: Out-of-fold predictive performance of the GPBoost speed model. Metrics are reported on both the transformed scale (training scale) and the original SOG (SOG) scale.

Scale	R^2	MAE	RMSE
Square Root Transform	0.798	0.331	0.475
Original SOG scale	0.770	1.035	1.767

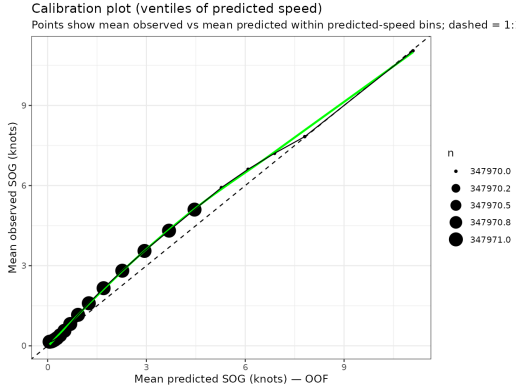


Figure 5: Out-of-fold calibration plot for the GPBoost model. Mean observed and predicted vessel speeds are compared across equal frequency bins of predicted SOG. The dashed line shows perfect calibration, and the smooth curve highlights systematic deviations.

5. Results

5.1. Binary Classification Results

Figure 6 summarizes the global importance of predictors in the classification model based on mean absolute SHAP values computed from out-of-fold predictions. Distance to coast was the most influential predictor, indicating that proximity to shore strongly determined whether a vessel was classified as having zero or positive SOG. Change in course over ground (Δ COG) and bathymetric depth ranked as the second and third most influential predictors, respectively. Here, Δ COG functioned as a steering indicator: small COG changes were associated with a higher probability of positive SOG, whereas large or frequent heading changes reduced the probability of positive SOG. Bathymetric depth contributed additional explanatory power, with vessels more likely to exhibit positive SOG in deeper waters than in shallow coastal regions. Vessel group and navigational status exhibited systematic effects on the probability of positive SOG, but their global contributions were modest

relative to distance to coast and ΔCOG . Wind along track, wind cross track, and sea ice concentration showed comparatively small mean absolute SHAP values, indicating limited average influence on zero versus positive SOG classification. Sine and cosine COG similarly showed low importance, suggesting that absolute heading direction played a minor role once proximity to shore and maneuvering intensity were accounted for.

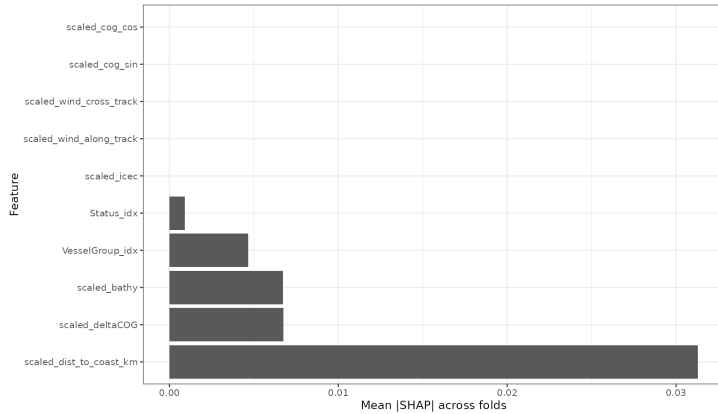


Figure 6: Global mean absolute SHAP values for the zero or positive SOG classification model. Larger values indicate greater average influence on the probability of positive SOG.

Across vessel groups (Figure 7), high speed craft exhibited the highest probability of positive SOG. Tug-Tow vessels were also more likely to be classified as having positive SOG than zero SOG. Dredgers, cruise ships, and unspecified vessel categories showed weak positive deviations from the model baseline, indicating mixed zero and positive SOG observations. In contrast, cargo vessels, tankers, fishing vessels, and service ships exhibited negative mean SHAP values, indicating that they were more frequently associated with zero SOG than positive SOG relative to the baseline. Pleasure craft

and vessels in the “other” category displayed similar negative contributions, reflecting intermittent positive SOG or prolonged periods of zero SOG.

Navigational status further differentiated zero versus positive SOG outcomes (Figure 8). Status 1 (at anchor) showed the strongest negative SHAP value, indicating an almost certain classification as zero SOG. Status 8 (underway sailing) and Status 2 (not under command) were also associated with reduced probability of positive SOG. In contrast, Status 0 (underway using engine) exhibited the strongest positive contribution, corresponding to a high likelihood of positive SOG. Statuses associated with active steering or transit such as Status 3 (restricted maneuverability), Status 12 (pushing ahead/towing alongside), and Status 15 (undefined/default) also contributed positively to the classification of positive SOG.

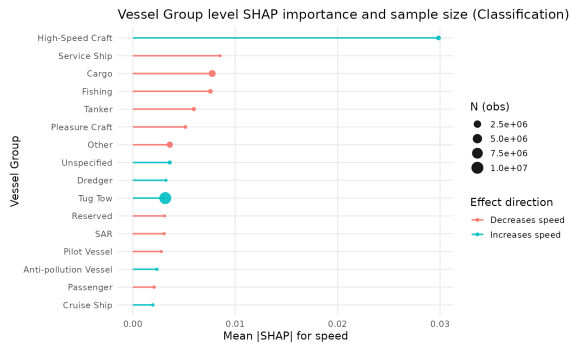


Figure 7: SHAP summary for the $\text{SOG} > 0$ classification model, showing the contribution of vessel group to positive SOG predictions.

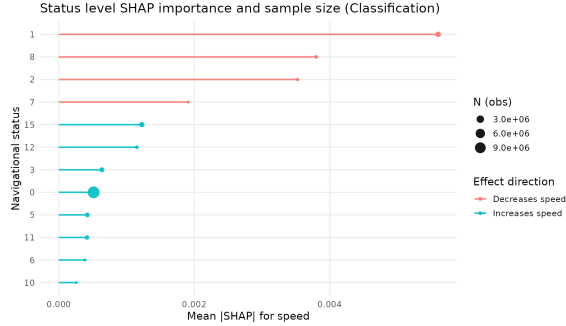


Figure 8: SHAP summary for the $\text{SOG} > 0$ classification model, showing the contribution of navigational status to positive SOG.

5.1.1. Marginal Effects of Key Covariates

SHAP values were reported on the latent probit scale, corresponding to the model’s linear predictor prior to transformation into probabilities. Distance to coast (Figure 9a) showed a strong nonlinear marginal effect on positive SOG probability. SHAP values were strongly negative within 2–3 km of shore, increased sharply between 5 and 30 km, and stabilized near zero to slightly positive beyond 40–50 km offshore, indicating diminishing influence in fully offshore environments. Change in course over ground (ΔCOG ; Figure 9b) showed a clear threshold effect on positive SOG probability. SHAP values were strongly positive for small heading changes ($\Delta\text{COG} < 5^\circ$), declined rapidly between 5° and 10° , and became persistently negative beyond 10° , indicating reduced likelihood of positive SOG during increased steering. Bathymetric depth (Figure 9c) showed a nonlinear effect on positive SOG probability, with near-zero to negative SHAP values in shallow waters, a pronounced minimum at intermediate depths, and a sharp increase to positive values beyond 180–200 m, indicating higher likelihood of positive SOG in deeper offshore waters.

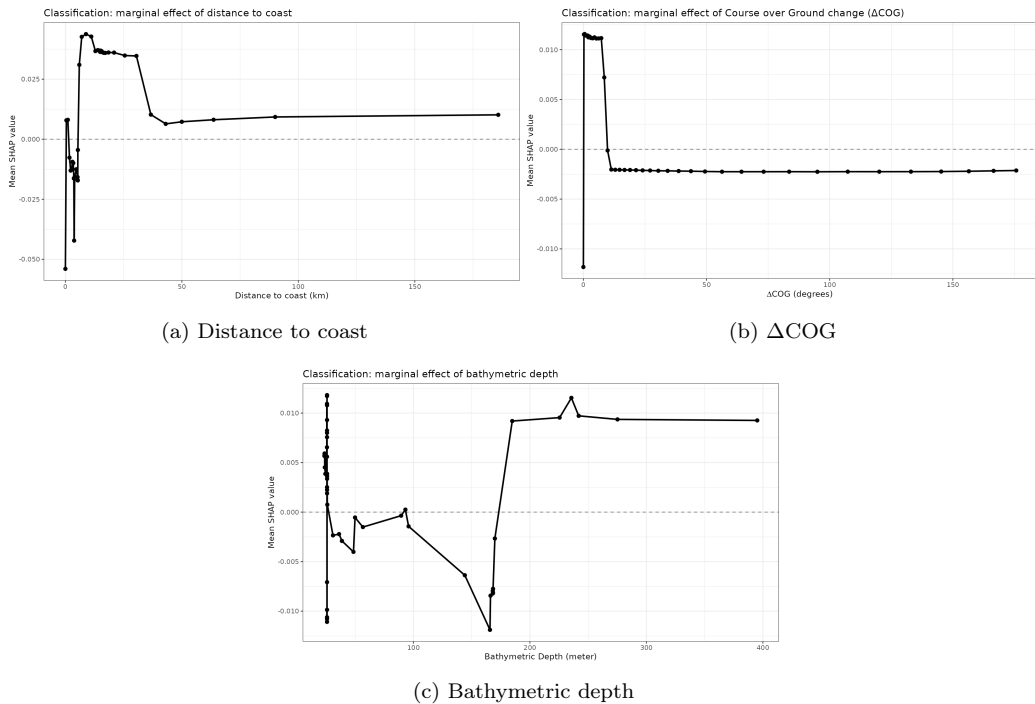


Figure 9: Marginal SHAP effects for key predictors in the SOG > 0 classification model. Panels show mean SHAP values on the probit scale across binned covariates for (a) distance to coast, (b) change in course over ground (ΔCOG), and (c) bathymetric depth. Positive SHAP values indicate an increased probability of positive vessel speed.

5.2. Positive Speed Regression Results

Vessel SOG regression model results showed that distance to coast emerged as the dominant predictor, indicating that spatial proximity to shore was the strongest determinant of vessel speed once vessels were underway. Change in course over ground (Δ COG) and bathymetric depth ranked second and third, respectively, highlighting the importance of navigational stability and seafloor constraints in shaping achievable speed. Directional components of COG, represented by sine and cosine encodings, exhibited moderate importance, indicating persistent directional effects on vessel speed while avoiding artificial discontinuities associated with angular variables. Their contribution was secondary to Δ COG. Operational attributes, including navigational status and vessel group, contributed additional explanatory power but were less influential than the primary spatial covariates mentioned above. Environmental variables wind along track, wind cross track, and sea ice concentration showed comparatively low mean absolute SHAP values.

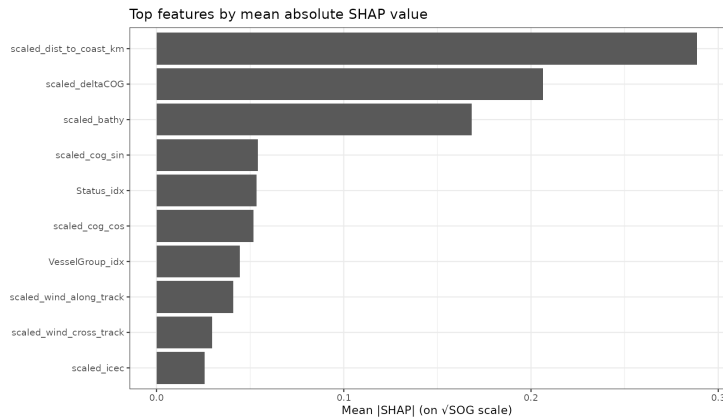


Figure 10: Global feature importance for the vessel speed regression model.

5.2.1. Covariate Marginal Effects on Vessel Speed

Distance to coast (Figure 11c) showed a strong nonlinear effect on predicted SOG, with low speeds nearshore (0 – 10 km), a rapid increase offshore (15 – 40 km), and stabilization beyond 50 – 60 km

Bathymetric depth (Figure 11b) showed a nonlinear positive effect on predicted vessel speed, with near-zero effects in shallow waters (0 – 50 m), a sharp increase at intermediate depths (80 – 150 m), and stabilization beyond 200 – 250 m, indicating diminishing influence in deeper offshore regions.

Change in course over ground (Δ COG; Figure 11a) showed a nonlinear effect on predicted vessel speed, with highest speeds for small heading changes ($< 5^\circ$), declining at moderate changes ($5 – 20^\circ$), and persistently lower speeds at larger changes, indicating reduced sustained speed during increased steering. Sea ice concentration and wind exhibited comparatively small marginal SHAP effects and are therefore not shown. Their limited influence reflected averaging across a wide range of operational contexts, including differences in vessel type, navigation status, and spatial setting. When other environmental, spatial, and operational variables were accounted for, ice and wind had a limited overall influence on vessel speed, although their effects may become more pronounced under specific ice or wind conditions. Navigational status exhibited clear, discrete influences on vessel speed (Figure 12), with both the direction and magnitude of effects varying substantially across operational states. Mean SHAP values for navigational status spanned a range from approximately -0.20 to $+0.06$ on the $\sqrt{\text{SOG}}$ scale. Negative SHAP values corresponded to reductions in predicted SOG relative to the model baseline, while positive values indicated increases. Status 10 (reserved; dangerous

goods/high speed craft) showed the strongest negative effect, with a mean SHAP value of approximately -0.20 , corresponding to a substantial reduction in predicted SOG. On the original SOG scale, this magnitude implied a meaningful decrease in SOG relative to baseline operating conditions. Other restrictive states, including Status 15 (not defined) and Status 5 (moored), exhibited smaller but consistent SOG reductions, with mean SHAP values on the order of -0.04 to -0.06 .

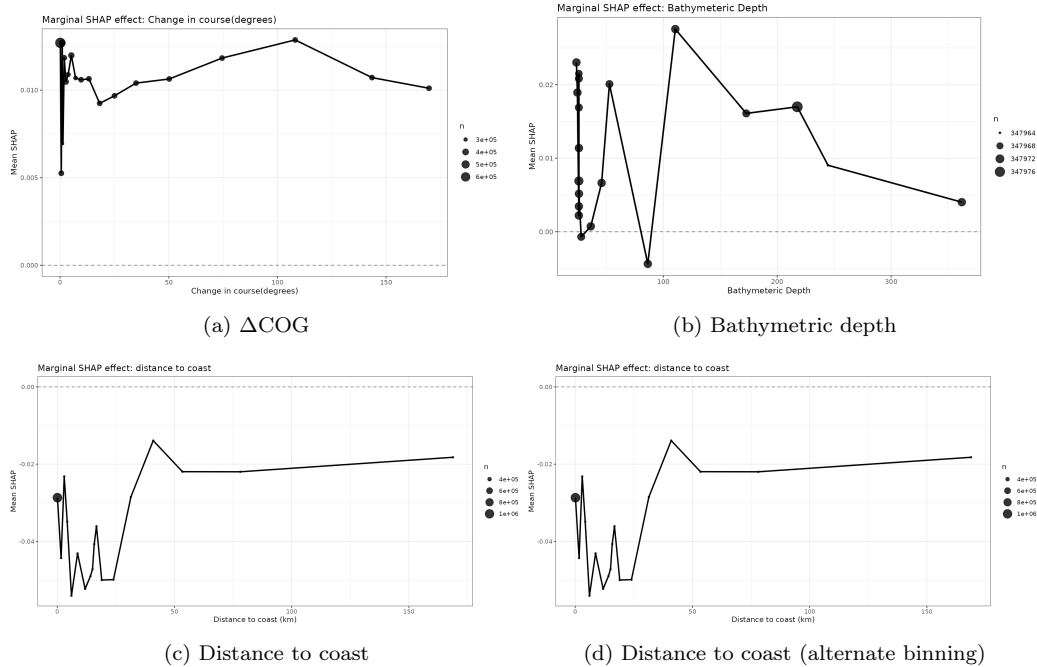


Figure 11: Marginal SHAP effects for key spatial and navigational predictors in the $\text{SOG} > 0$ regression model. Panels show mean SHAP values (on the $\sqrt{\text{SOG}}$ scale) across binned covariates for (a) change in course over ground (ΔCOG), (b) bathymetric depth, (c) distance to coast, and (d) an alternative binning of distance to coast. Marker size reflects bin sample size.

In contrast, Status 6 (aground), Status 7 (engaged in fishing), and Status 12 (pushing ahead/towing alongside) displayed positive mean SHAP val-

ues of approximately $+0.04$ to $+0.06$, indicating increased predicted SOG conditional on positive SOG. These positive contributions suggested that, when vessels were actively navigating under these statuses, higher SOG were more frequently observed relative to the baseline. By comparison, common navigational states such as underway using engine (Status 0), at anchor (Status 1), and restricted maneuverability (Status 3) clustered tightly around zero, with mean SHAP magnitudes generally below 0.02, indicating minimal marginal influence on SOG once other covariates were accounted for.

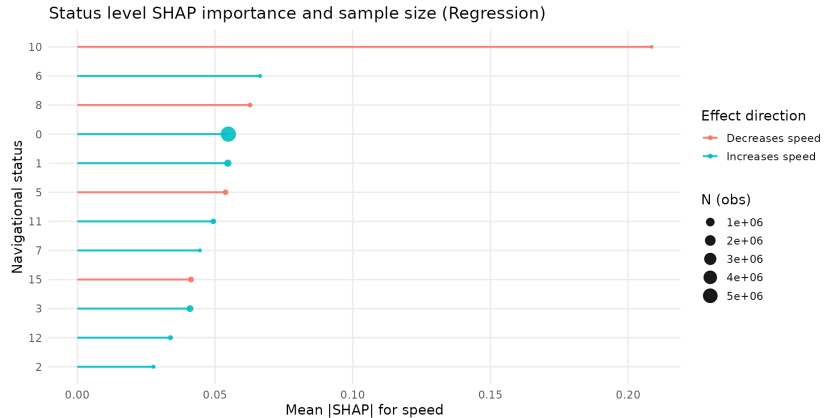


Figure 12: SHAP summary for the $\text{SOG} > 0$ regression model, showing the effect of navigation status on predicted vessel speed.

Figure 13 showed systematic differences in baseline vessel SOG across vessel groups, with mean SHAP values ranging approximately from -0.06 to $+0.18$ on the $\sqrt{\text{SOG}}$ scale. Positive SHAP values indicated vessel groups that tended to operate at higher SOG relative to the model baseline, while negative values indicated systematically lower SOG.

Passenger vessels and tankers exhibited the largest positive contributions, with mean SHAP values of approximately $+0.15$ to $+0.18$, corresponding to

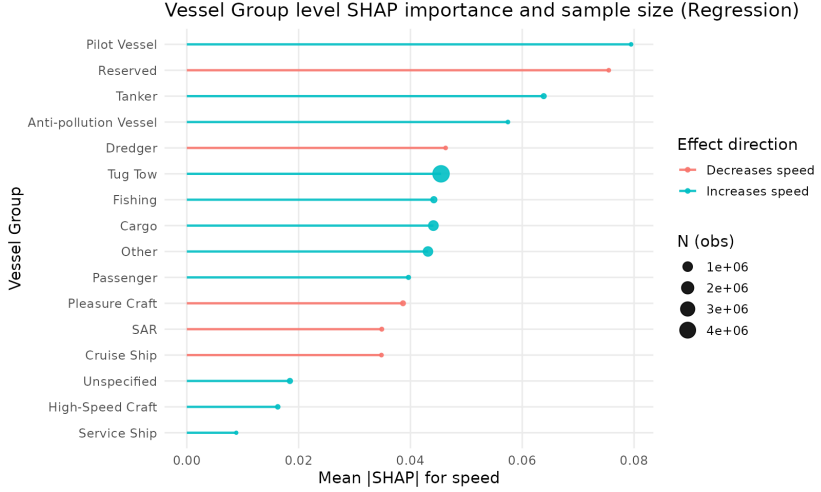


Figure 13: SHAP summary for the $\text{SOG} > 0$ regression model, showing the effect of vessel group on predicted vessel speed.

substantial increases in predicted SOG. Pilot vessels and tug-tow operations also showed strong positive effects, with mean SHAP values on the order of +0.10 to +0.15.

Cargo, fishing, and other general purpose vessels displayed more moderate SOG increases, with mean SHAP values typically between +0.05 and +0.08. In contrast, cruise ships, dredgers, anti-pollution vessels, and pleasure craft were associated with negative mean SHAP values, generally ranging from -0.03 to -0.06, indicating systematic reductions in vessel SOG. Overall, vessel group imposed a strong structural constraint on achievable SOG, with effect magnitudes that exceeded those of individual environmental covariates and persisted across a wide range of operating conditions.

6. Discussion

By explicitly distinguishing zero speed from positive speed regimes, this study enabled a targeted interpretation of where and when speed related risks arose in the U.S. Arctic. Nearshore regions characterized by frequent zero speed activity were associated with increased steering, congestion, and prolonged vessel presence, whereas offshore transit corridors were primarily associated with sustained higher speeds. These nearshore operating regimes often overlapped with ecologically sensitive coastal habitats and marine mammal use areas documented in prior studies (Reeves et al., 2014; Hauser et al., 2018; Halliday et al., 2017), indicating that navigational and ecological risks may co-occur in space. Together, these findings showed that speed related risk in Arctic waters was strongly context dependent.

Across both modeling stages, spatial context captured primarily by distance to coast emerged as the dominant determinant of vessel SOG. Very close to shore, the probability of positive SOG was substantially reduced, while both the likelihood and magnitude of vessel speed increased rapidly offshore before stabilizing at greater distances. This pattern was consistent with AIS based studies documenting concentrated low speed and zero speed activity in coastal operating regions and more stable transit behavior offshore (Ma et al., 2024). These results indicated that proximity to shore governed both whether vessels moved and how fast they traveled when underway.

Changes in course over ground (Δ COG), provided a complementary distinction between operating regimes. Small heading changes were associated with sustained transit and higher speeds, whereas large or frequent directional changes corresponded to reduced speed and a lower probability of

positive SOG. Similar patterns had been documented in AIS-based studies of maneuvering intensive activities, where frequent course changes reflected localized operations rather than long distance transit (Xing et al., 2023). Together, distance to coast and ΔCOG distinguished corridor based navigation from maneuvering dominated regimes in a way not captured by static vessel attributes alone.

Bathymetric depth further contributed to both classification and regression outcomes. Shallow waters were associated with a higher probability of zero-speed observations, while deeper waters supported higher and more stable transit speeds. This finding aligned with prior AIS analyses showing systematic differences in vessel behavior between shallow coastal environments and deeper offshore regions, where navigational constraints were reduced and maneuvering intensity was lower (Ma et al., 2024).

Operational characteristics such as vessel group and navigational status introduced systematic but secondary variation in vessel speed behavior (see supplementary figure S1,S7 and S8). Status codes indicating anchoring or mooring were strongly associated with zero SOG, while transit related statuses corresponded to positive SOG, consistent with AIS definitions. Vessel group effects similarly reflected operational roles observed in the data. However, across both classification and regression models, these operational attributes did not override the dominant influence of spatial setting and steering behavior (see supplementary figure S2,S9 and S10), as reflected in global SHAP rankings where distance to coast and ΔCOG consistently exceeded vessel group and status in explanatory importance.

Environmental variables, including wind speed and sea ice concentration,

exhibited modest average influence on vessel SOG because their effects were highly nonlinear and strongly context dependent (see Supplementary Material Figure S3, S4, S6 and S7). When summarized using global SHAP measures, impacts arising only under specific conditions such as high ice concentration, adverse winds, or constrained navigation were attenuated by averaging across heterogeneous vessels, routes, and predominantly open-water conditions during the July–October season. Consequently, wind and ice could exert substantial localized influence in particular operating regimes even though their global importance appeared limited. This interpretation was consistent with prior work showing that wind and ice effects became dominant only under specific operating conditions (Aksenov et al., 2017; Montewka et al., 2015).

A key implication of the two-stage framework was that it separated operating regimes that were conflated in single-stage speed models. When SOG was modeled as a single continuous response, zero speed observations dominated nearshore and steering intensive contexts, biasing predicted speeds downward and obscuring transitions between stationary behavior and sustained transit. In contrast, the two-stage structure first identified whether a vessel was likely to be underway ($\text{SOG} > 0$) and then modeled achievable speed conditional on transit. This decomposition allowed speed suppression near the coast to be interpreted as a combination of increased stopping and reduced conditional speed rather than as a single averaged effect. As a result, the model outputs provided a clearer operational distinction between areas dominated by steady or steering and corridors where sustained transit at higher speeds was feasible.

From an operational standpoint, this distinction helped identify where

speed management efforts would be most effectively focused, including reducing stop-and-go congestion in nearshore corridors versus moderating sustained transit speeds in offshore routes.

Although the two-stage framework improved interpretability, AIS-reported SOG and navigational status may have contained measurement noise, and environmental covariates mapped at daily $0.5^\circ \times 0.5^\circ$ resolution may have smoothed localized extremes. The analysis was limited to the July–October season and excluded drivers such as ocean surface currents, which can substantially influence SOG (Zhou et al., 2020; Yang et al., 2020) and contribute to unexplained variability, particularly in coastal corridors. Future work could address these limitations by incorporating higher-resolution environmental data, extending analyses to additional seasons, and explicitly accounting for AIS measurement uncertainty.

References

- Aksenov, Y., Popova, E.E., Yool, A., Nurser, A.J.G., Williams, T.D., Bertino, L., Bergh, J., 2017. On the future navigability of arctic sea routes: high-resolution projections of the arctic ocean and sea ice. *Marine Policy* 75, 300–317. doi:10.1016/j.marpol.2015.12.027.
- Chang, K.Y., He, S.S., Chou, C.C., Kao, S.L., Chiou, A.S., 2015. Route planning and cost analysis for travelling through the arctic northeast passage using public 3D GIS. *Geogr. Inf. Syst.* 29, 1375–1393.
- Chen, T., Guestrin, C., 2016. Xgboost: A scalable tree boosting system, in: *Proceedings of the 22nd ACM SIGKDD International Conference on Knowledge Discovery and Data Mining*, ACM. pp. 785–794. doi:10.1145/2939672.2939785.
- Copernicus Climate Change Service (C3S), 2024. Era5 post-processed daily-statistics on single levels from 1940 to present. doi:10.24381/cds.4991cf48. accessed on 28-Sep-2025.
- Feinstein, A.R., Cicchetti, D.V., 1990. High agreement but low kappa: I. the

- problems of two paradoxes. *Journal of Clinical Epidemiology* 43, 543–549. doi:10.1016/0895-4356(90)90158-L.
- Goerlandt, F., Montewka, J., Zhang, W., Kujala, P., 2017. An analysis of ship escort and convoy operations in ice conditions. *Saf. Sci.* 95, 198–209.
- Halliday, W.D., Insley, S.J., Hilliard, R.C., de Jong, T., Pine, M.K., 2017. Potential impacts of shipping noise on marine mammals in the western canadian arctic. *Marine Pollution Bulletin* 123, 73–82. doi:10.1016/j.marpolbul.2017.09.027.
- Hauser, D.D.W., Laidre, K.L., Stern, H.L., Moore, S.E., Suydam, R.S., 2018. Habitat selection by two beluga whale populations in the chukchi and beaufort seas. *PLOS ONE* 13, e0203657. doi:10.1371/journal.pone.0203657.
- HSVA Arctic Technology, 2014. Calculation of fuel consumption per mile for various ship types and ice conditions in past, present and in future. Technical Report D2.42. ACCESS Arctic Climate Change, Economy and Society, Seventh Framework Programme (Project #265863). Figure 8: Speed of ship depending on ice concentration.
- Huang, B., Liu, C., Banzon, V., Freeman, E., Graham, G., Hankins, B., Smith, T., Zhang, H.M., 2021. Improvements of the daily optimum interpolation sea surface temperature (doisst) version 2.1. *Journal of Climate* 34, 2923–2939. doi:10.1175/JCLI-D-20-0166.1.
- Japkowicz, N., Stephen, S., 2002. The class imbalance problem: A systematic study. *Intelligent Data Analysis* 6, 429–449.
- Ke, G., Meng, Q., Finley, T., Wang, T., Chen, W., Ma, W., Ye, Q., Liu, T.Y., 2017. Lightgbm: A highly efficient gradient boosting decision tree, in: *Advances in Neural Information Processing Systems*, pp. 3146–3154.
- Kuuliala, L., Kujala, P., Suominen, M., Montewka, J., 2017. Estimating operability of ships in ridged ice fields. *Cold Reg. Sci. Technol.* 135, 51–61.
- Löptien, U., Axell, L., 2014. Ice and AIS: ship speed data and sea ice forecasts in the baltic sea. *Cryosphere* 8, 2409–2418.
- Lundberg, S.M., Lee, S.I., 2017. A unified approach to interpreting model predictions, in: *Advances in Neural Information Processing Systems*, Curran Associates, Inc.
- Ma, L., Guo, Z., Shi, G., 2024. Ais data driven ship behavior modeling in fair-

- ways: A random forest based approach. *Applied Sciences* 14. URL: <https://www.mdpi.com/2076-3417/14/18/8484>, doi:10.3390/app14188484.
- Montewka, J., Goerlandt, F., Kujala, P., Lensu, M., 2015. Towards probabilistic models for the prediction of a ship performance in dynamic ice. *Cold Reg. Sci. Technol.* 112, 14–28.
- Pruyn, J.F.J., 2016. Will the northern sea route ever be a viable alternative? *Marit. Policy Manage.* 43, 661–675.
- Reeves, R.R., Ewins, P.J., Agbayani, S., Heide-Jørgensen, M.P., Kovacs, K.M., Lydersen, C., Suydam, R., Elliott, W., Polet, G., van Dijk, Y., Blijlevens, R., 2014. Distribution of endemic cetaceans in relation to hydrocarbon development and commercial shipping in the canadian arctic. *Marine Policy* 44, 375–389. doi:10.1016/j.marpol.2013.10.005.
- Sigrist, F., 2021. Gaussian process boosting. doi:10.48550/arXiv.2004.02653.
- U.S. Committee on the Marine Transportation System, 2019. A Ten-Year Projection of Maritime Activity in the U.S. Arctic Region, 2020–2030. Technical Report. U.S. Committee on the Marine Transportation System. Washington, D.C.
- Wang, J., Guo, Y., Wang, Y., 2022. A sequential random forest for short-term vessel speed prediction. *Ocean Engineering* 248, 110691. URL: <https://www.sciencedirect.com/science/article/pii/S0029801822001470>, doi:<https://doi.org/10.1016/j.oceaneng.2022.110691>.
- Wikle, C.K., Datta, A., Hari, B.V., Boone, E.L., Sahoo, I., Kavila, I., Castruccio, S., Simmons, S.J., Burr, W.S., Chang, W., 2023. An illustration of model agnostic explainability methods applied to environmental data. *Environmetrics* 34, e2772.
- Xing, B., Zhang, L., Liu, Z., Sheng, H., Bi, F., Xu, J., 2023. The study of fishing vessel behavior identification based on ais data: A case study of the east china sea. *Journal of Marine Science and Engineering* 11. URL: <https://www.mdpi.com/2077-1312/11/5/1093>, doi:10.3390/jmse11051093.
- Yang, L., Chen, G., Zhao, J., Rytter, N.G.M., 2020. Ship speed optimization considering ocean currents to enhance environmental sustainability in maritime shipping. *Sustainability* 12. URL: <https://www.mdpi.com/2071-1050/12/9/3649>, doi:10.3390/su12093649.

- Yang, Y., Liu, Y., Li, G., Zhang, Z., Liu, Y., 2024. Harnessing the power of machine learning for ais data-driven maritime research: A comprehensive review. *Transportation Research Part E: Logistics and Transportation Review* 183, 103426. URL: <https://www.sciencedirect.com/science/article/pii/S1366554524000164>, doi:<https://doi.org/10.1016/j.tre.2024.103426>.
- Zhou, Y., Daamen, W., Vellinga, T., Hoogendoorn, S.P., 2020. Impacts of wind and current on ship behavior in ports and waterways: A quantitative analysis based on ais data. *Ocean Engineering* 213, 107774. URL: <https://www.sciencedirect.com/science/article/pii/S0029801820307514>, doi:<https://doi.org/10.1016/j.oceaneng.2020.107774>.

Appendix A.

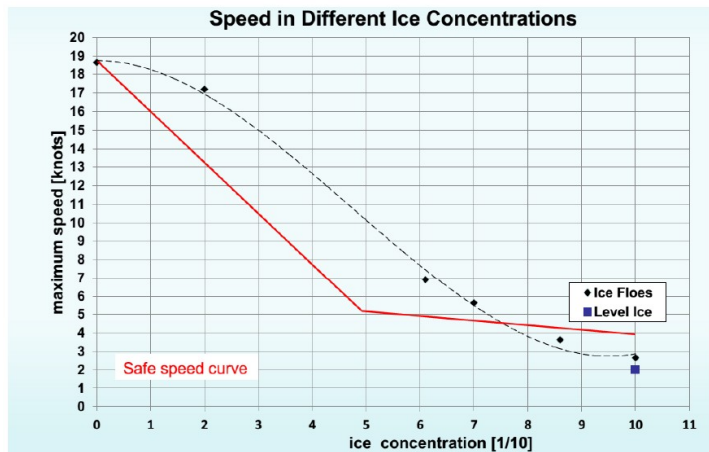


Figure A1: Maximum recommended vessel speed as a function of sea ice concentration. Black symbols and dashed curves show observed speed–ice relationships, while the solid red line denotes the conservative safe speed threshold used to define ice-related navigation risk. Ice concentration is expressed in tenths (0–10) and speed in knots. Adapted from ACCESS ship performance guidance (HSVA Arctic Technology, 2014).